

Turning Agricultural Waste into a Powerful Solution: Enhanced Lead Removal via Chemically Modified Oat Straw

JELENA DIMITRIJEVIĆ^{1*}, SANJA JEVTIĆ², MARIJA SIMIĆ¹, MARIJA KOPRIVICA¹, ALEKSANDAR JOVANOVIĆ¹, MILICA MIŠIĆ¹ AND JELENA PETROVIĆ¹

¹Institute for Technology of Nuclear and Other Mineral Raw Materials, 86 Franchet d'Esperey St., 11000 Belgrade, Serbia;

²Faculty of Technology and Metallurgy, University of Belgrade, 4 Carnegie, 11000 Belgrade, Serbia

*Corresponding author: j.dimitrijevic@itnms.ac.rs

Received: October 29, 2024

Accepted: November 12, 2024

Published on-line: December 23, 2024

Published: December 25, 2024

The release of industrial effluents and agricultural runoff containing heavy metals, like lead (Pb), poses serious environmental risks and significant impact on human health. This study explores the adsorption capacity of potassium hydroxide (KOH)-modified oat straw (KOS) as an effective, low-cost biosorbent for lead removal from contaminated water. The modification process increased the surface area and improved the availability of functional groups, enhancing adsorption performance compared to unmodified oat straw. Structural analysis was conducted using Scanning Electron Microscopy (SEM) and Fourier Transform Infrared spectroscopy (FTIR). Batch experiments evaluated the effects of contact time, initial Pb²⁺ concentration, and pH on lead removal efficiency. The adsorption process followed pseudo-second-order kinetics, with chemisorption as the main mechanism. Isotherm studies indicated that the Langmuir and Redlich-Peterson models offered the best fit, showing a maximum adsorption capacity of 191.41 mg/g. These findings highlight the potential of KOH-modified oat straw as a sustainable solution for heavy metal removal from wastewater, effectively valorizing agricultural waste biomass.

Keywords: *Avena sativa* L; biomass; heavy metals; wastewater treatment; adsorption, ecofriendly process

<https://doi.org/10.61652/leksir2444011D>

1. INTRODUCTION

The release of industrial effluents and agricultural run-off into water bodies has resulted in significant global concerns regarding water pollution. Pollutants like heavy metals, dyes, pesticides, and pharmaceuticals have a profound impact on the environment, causing risks to human health, animals, and ecosystems (Dimitrijević et al., 2023; Jovanović et al., 2023; Simić et al., 2022). Due to their persistence, non-degradability, and high toxicity even at low concentrations, heavy metals in particular, such as Pb, cadmium (Cd), and mercury (Hg), represent a critical threat (Zhang et al., 2022). These metals accumulate in living organisms, leading to serious health risks. For this reason, finding effective methods to treat wastewater before its discharge into the environment has become an urgent priority.

Various conventional methods, including coagulation, flocculation, membrane filtration, and chemical precipitation, have been employed to treat wastewater. However, these methods often face limitations such as high operational costs, complexity, and inefficiency in removing pollutants at low concentrations

(Dimitrijević et al., 2023; Simić et al., 2022; Zhang et al., 2022).

As a result, there is a growing interest in more sustainable and efficient solutions, particularly in the form of biosorbents.

Adsorption has emerged as a highly selective, efficient, and cost-effective technique for removing pollutants from water (Gollakota et al., 2022). Over the past few decades, the application of natural materials, particularly agricultural waste, has gained significant attention due to its sustainability, availability, and low cost (Borrega et al., 2022). Agricultural residues like oat straw, waste coffee pulp, corn cob, and banana pseudo-stems have been investigated for their potential use as biosorbents due to their abundance and renewable nature (Dimitrijević et al., 2023; Fan et al., 2022). Biomass materials are particularly attractive because they contain functional groups, such as carboxyl, phenolic, and amine groups, which interact with pollutants through mechanisms such as hydrogen bonding and electrostatic interactions (Fan et al., 2022). To improve the adsorption capacity of biosorbents, chemical modifications are often per-

formed. Alkali treatments, with KOH are commonly used to enhance the surface area and introduce additional binding sites. For example, Simić et al. (2022) demonstrated that KOH modification of corn silk increased its capacity to remove cadmium Cd (II) ions by more than twofold.

In this context, we explore oat straw, a low-cost byproduct left after oat harvesting, which is available in large quantities. Oat (*Avena sativa* L.) is well known as a quality source of antioxidants such as E-vitamins (α and β tocopherol, α and β tocotrienol), free or esterified phenolic acids (e.g. *p*-coumaric, caffeic and ferulic acids) and avenanthramides (avenanthramides 1, 3, and 4) (Bryngelsson et al., 2002; Ren et al., 2011). These phenols exhibit antioxidant, anti-inflammatory, and anti-proliferative activity, which distinguishes this plant as very useful (Kim et al., 2021). Additionally, oat compounds have shown benefits in reducing hyperglycemia, hyperinsulinemia, hypercholesterolemia, and hypertension (Dong et al., 2011). Despite its potential, oat straw remains largely underutilized, making it an ideal candidate for valorization. The lignocellulosic composition of oat straw includes cellulose, hemicellulose, and lignin, providing multiple active sites for adsorption (Gómez Aguilar et al., 2020). While previous studies have investigated oat husks, there is a gap in the research regarding the potential of oat straw itself as a biosorbent. Its composition also includes minerals like magnesium, calcium, and sodium, which enhance its ion-exchange capacity, making it particularly effective for heavy metals like Pb (Hatiya et al., 2022).

In this study, we have focused on modifying oat straw using potassium hydroxide (KOH), a practical and cost-effective treatment. Our primary objective is to evaluate the efficacy of KOH-modified oat straw in adsorbing Pb from contaminated water, given the frequent presence of lead in industrial effluents and its lethal effects on human health. The second objective lies in the potential to turn a widely available agricultural byproduct into an efficient biosorbent for environmental remediation (Kosiorek and Wyszowski, 2019). This approach offers a scalable, environmentally friendly option for treating contaminated water while simultaneously addressing pollution and waste management challenges.

2. MATERIALS AND METHODS

2.1. Chemicals

All chemicals and reagents used in this study were of analytical purity. Lead nitrate ($\text{Pb}(\text{NO}_3)_2$) was used to prepare stock solutions (1000 mg/L) for the adsorption tests. The stock solutions were diluted with ultra-distilled water to achieve desired working concentrations. KOH was utilized for the chemical modification of the biosorbent.

2.2. Biomass Preparation

Oat straw waste was used as the base biomass material, collected from a local field in Banat, Serbia, after the 2021 harvest. The biomass was thoroughly washed to remove any remaining soil and surface impurities, air-dried at room temperature, and then ground and sieved to obtain a particle size fraction of 63-125 μm . The material was subsequently oven-dried at 105 °C to a constant weight. For the chemical modification process, the prepared OS was treated with KOH to improve its adsorptive properties by modifying its surface structure, specifically targeting hemicellulose breakdown. The modified biomass (KOS) was stored in sealed containers for further use in the adsorption experiments.

2.3. Biomass Modification

The modification of the OS biosorbent was carried out by treating 2 g of the raw material with 50 mL of 0.1 mM potassi-

um hydroxide (KOH) solution (Petrović et al., 2016). The mixture was stirred on a magnetic stirrer for 4 hours to ensure thorough interaction between the KOH and the biomass. After the reaction, the modified biomass was filtered through filter paper, and the residue was rinsed with distilled water until the filtrate reached a neutral pH of 7, effectively removing any excess KOH remaining on the material surface. The neutralized biomass was then dried and stored for further adsorption experiments and characterization.

2.4. Biomass Characterization

To evaluate the structural changes resulting from the modification process, a detailed characterization of both OS and KOS samples was conducted. Surface analysis was performed using Fourier Transform Infrared (FTIR) spectroscopy on a Thermo Scientific Nicolet iS50 FT-IR spectrometer. The samples were prepared by mixing 0.8 mg of either OS or KOS with 80 mg of KBr, and the spectra were recorded within the range of 4000 to 400 cm^{-1} .

The structural properties of the biosorbents were examined using Scanning Electron Microscopy (SEM) on a MIRA TESCAN microscope, operating at 20 keV. Before imaging, all samples were coated with a thin layer of gold, and mounted on adhesive carbon discs to ensure conductivity during analysis.

2.5. Adsorption Studies

To understand the impact of the modification process on the efficiency of the adsorbent, a preliminary adsorption test was conducted using both materials. For the test, 0.1 g/L of each biosorbent was added to a 1 mM Pb solution. The contact time was 24 hours, after which the concentration of remaining lead ions in the filtrates was measured by Atomic Absorption Spectrophotometry (AAS) at Perkin Elmer 900T.

Further adsorption studies were conducted using KOS as the adsorbent to optimize adsorption conditions and investigate the Pb^{2+} removal mechanism. Several key operational parameters were varied, including the initial pH of the solution (2-5), contact time (15-1440 min), and initial concentration of lead ions (40-400 mg/L). Adsorption experiments were carried out using a sorbent dose of 1 g/L and a lead solution at pH 5.

The batch adsorption experiments were performed in 100 mL Erlenmeyer flasks and placed on an orbital shaker at 220 rpm and room temperature. After the specified contact time, the remaining concentration of lead ions in the solution was measured using AAS.

The amount of lead adsorbed onto the biosorbent was calculated using the following equation:

$$q_e = \frac{(C_i - C_e) \cdot V}{m} \quad (1)$$

where: q_e is the amount of lead adsorbed (mg/g), C_i and C_e are the initial and equilibrium concentrations of lead (mg/L), V is the volume of the solution (L), m is the mass of the adsorbent (g).

Adsorption kinetics and isotherm models were evaluated using both linear and non-linear fitting methods with Origin software. Additionally, to investigate the potential ion-exchange mechanism during lead adsorption, the concentrations of released cations (such as Ca^{2+} , Mg^{2+} , K^+ , Na^+) were monitored after adsorption by AAS.

3. RESULTS

3.1. Material Characterization

3.1.1. SEM

SEM was employed to closely examine the morphological

changes in OS and KOS. The SEM micrograph of native OS (Figure 1a) reveals a smooth, continuous surface characteristic of untreated lignocellulosic biomass (Dimitrijević et al., 2023). Notably, well-defined channels and occasional cracks are observed across the surface, which is typical for plant-based structures (Simić et al., 2022). These features suggest that the native OS has limited surface area and adsorption capacity due to its relatively unaltered and compact structure. Following modification with KOH, significant morphological transformations are evident, as shown in the SEM image of KOS (Figure 1b).

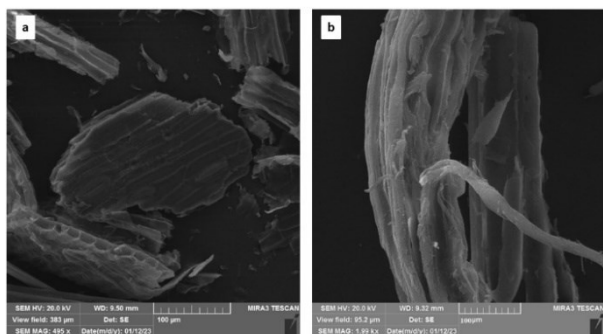


Fig. 1: SEM micrographs of OS (a) and KOS (b)

The previously smooth surface becomes highly disordered, with numerous cracks, channels, and rough textures (Lai et al., 2023). This pronounced surface disruption is indicative of the chemical action of KOH, which likely leads to partial degradation of cellulose and hemicellulose components within the lignocellulosic matrix. Such degradation results in the formation of new surface pores and an overall increase in surface roughness, thereby creating a more porous structure (Gollakota et al., 2022).

The increase in surface heterogeneity and the formation of additional microchannels in KOS are crucial for enhancing the adsorption properties of the material. The new cracks and pores provide improved pathways for ion diffusion, facilitating greater interaction between the material's active sites and metal ions in solution. This observation aligns with previous research, which has demonstrated that chemical modifications, such as alkaline treatments, significantly improve the adsorption performance of biomass by increasing the number of accessible binding sites (Dimitrijević et al., 2023; Gollakota et al., 2022).

3.1.1. FTIR Analysis

To investigate the chemical structure changes in native OS caused by KOH modification, FTIR analysis was conducted, and the spectra before and after modification are shown in Figure 2. The FTIR spectrum of OS exhibits characteristic peaks for lignocellulosic biomass. The broad peak around 3300 cm^{-1} is attributed to O-H stretching vibrations from hydroxyl groups as expected for cellulose and hemicellulose (Babicka et al., 2022; Lawal et al., 2017). After modification with KOH, this peak diminishes, indicating a reduction in free hydroxyl groups due to their participation in chemical reactions.

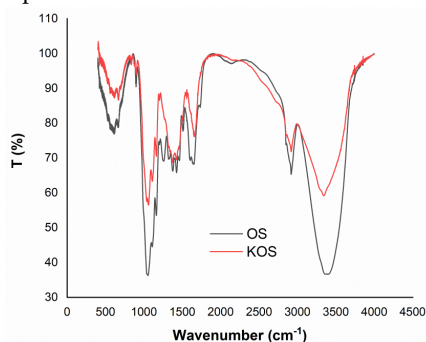


Fig. 2: FTIR spectra of OS and KOS

The peak around 2918 cm^{-1} , associated with C-H stretching vibrations from cellulose and hemicellulose, also decrease after modification, suggesting partial degradation of hemicellulose. This is further supported by changes in the region between 1000 and 1100 cm^{-1} , where C-O-C stretching vibrations occur (Dehkhoda et al., 2022; Kubovský et al., 2020). The shift and weakening of these peaks in the KOS spectrum confirm structural alterations in the ether bonds of cellulose and hemicellulose, likely enhancing the material's adsorption capacity.

Additionally, the peaks around 1600–1650 cm^{-1} , corresponding to C=O stretching in lignin and cellulose, are less pronounced in the KOS spectrum, suggesting modifications in the carbonyl groups. In the region between 500 and 800 cm^{-1} , the increase in intensity points to the possible incorporation of new functional groups or minerals after KOH treatment, which could play a role in enhancing ion exchange properties (Lawal et al., 2017; Ying et al., 2017).

In summary, the FTIR analysis confirms significant structural changes in OS after modification with KOH. These changes, including the reduction of hydroxyl groups and degradation of hemicellulose, contribute to the improved adsorptive properties of KOS (Simić et al., 2022).

In addition, FTIR analysis was performed to identify the structural changes in KOS before and after Pb adsorption. The broad peak around 3300 cm^{-1} , corresponding to O-H stretching, shows a decrease in intensity after Pb²⁺ adsorption (KOS-Pb), indicating the interaction between lead ions and hydroxyl groups on the biosorbent surface. The C-H stretching vibrations at 2918 cm^{-1} , associated with cellulose and hemicellulose, also decrease in intensity, suggesting that these components may be affected by lead binding. The C=O stretching vibrations around 1600–1650 cm^{-1} , which represent carbonyl groups of lignin and cellulose, show reduced intensity after adsorption, implying their involvement in the adsorption process (Lawal et al., 2017; Ying et al., 2017). In the C-O-C stretching region (1000–1100 cm^{-1}), slight shifts and a reduction in peak intensity suggest structural changes in the cellulose and hemicellulose ether linkages. Furthermore, the increased intensity in the 500–800 cm^{-1} region after Pb²⁺ adsorption points to the possible formation of new bonds or interactions with lead ions (Petrović et al., 2023).

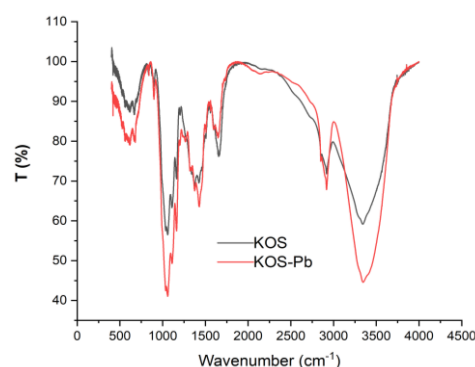


Fig. 3: FTIR spectra of KOS before and after Pb²⁺ adsorption

Overall, the FTIR spectra reveal that lead adsorption on KOS involves interactions with hydroxyl, carbonyl, and ether groups, confirming the role of both chemisorption and ion exchange in the adsorption mechanism (Petrović et al., 2016; Simić et al., 2022).

3.2. Batch adsorption tests

3.2.1. Preliminary Adsorption Test

The preliminary adsorption test was performed to evaluate the effectiveness of OS and KOS in removing Pb from aqueous

solutions. The biosorbent OS, showed an adsorption capacity of 38 mg/g, while the KOS, showed a significantly higher capacity of 89 mg/g. This clear increase in performance highlights the effectiveness of the KOH modification, which enhances the biosorbent's surface properties and provides more active sites for lead binding. Due to this substantial improvement, all subsequent adsorption studies were carried out using the modified KOS biosorbent to ensure optimal results.

3.2.2. Influence of Contact Time and Kinetic Studies

The impact of contact time on the adsorption of Pb ions by the KOS was investigated to establish the equilibrium time for sorption. The decrease in Pb ion concentration was observed over a time period ranging from 15 to 1440 minutes. As shown in Figure 4, the adsorption process began rapidly, with approximately 50% of lead ions being removed within the first 60 minutes. This fast initial uptake can be attributed to the abundance of accessible active sites on the KOS surface, where lead ions quickly interacted with these sites (Dimitrijević et al., 2023; Petrović et al., 2016).

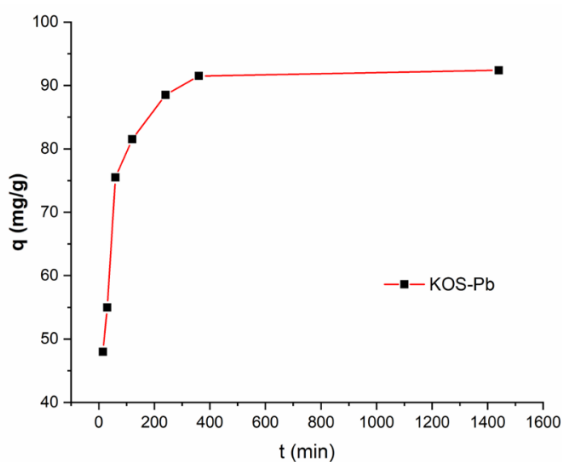


Fig. 4: Effect of contact time on Pb adsorption on KOS

After this initial period, the rate of adsorption slowed down, and the adsorption capacity gradually increased until equilibrium was reached. The equilibrium capacity for Pb²⁺ adsorption was found to be 93.45 mg/g, with equilibrium being achieved after approximately 240 minutes. This behavior suggests that after the rapid adsorption phase, the remaining unoccupied sites required more time for diffusion and interaction with the lead ions, likely due to intraparticle diffusion limitations (Petrović et al., 2016).

3.2.3. Adsorption Kinetic Study

Kinetic studies provide valuable information on the adsorption mechanisms, the rate of sorption, and potential rate-limiting steps. To interpret the kinetics of Pb²⁺ adsorption on KOS, three models were applied: the pseudo-first-order model (Lagergren, 1898), the pseudo-second-order model (Ho and McKay, 1999), and the Weber-Morris intraparticle diffusion model (Weber and Morris, 1963). These models help elucidate whether the process is controlled by physical adsorption, chemical adsorption (chemisorption), or diffusion mechanisms. The pseudo-first-order model, based on the assumption that the rate of adsorption is proportional to the number of available adsorption sites, is described by the equation:

$$\frac{1}{q_t} = \left(\frac{k_1}{q_{eq}} \right) \left(\frac{1}{t} \right) + \left(\frac{1}{q_{eq}} \right) \quad (2)$$

where: q_{eq} is the equilibrium adsorption capacity (mg/g), q_t is the amount of adsorbate adsorbed at time t

(mg/g), and k_1 is the pseudo-first-order rate constant (1/min). In this study, the pseudo-first-order model provided a poor fit to the experimental data, with a low correlation coefficient, indicating that the adsorption of lead onto the biosorbent is not primarily controlled by physical adsorption (Table 1). This suggests that the interaction between the lead ions and the biosorbent surface involves more complex mechanisms, such as chemical bonding, which is better captured by other models. The pseudo-second-order kinetic model assumes that chemisorption is the rate-limiting step in the adsorption process. This model is represented by the equation:

$$\frac{t}{q_t} = \left(\frac{1}{k_2 q_{eq}^2} \right) + \left(\frac{1}{q_{eq}} \right) t \quad (3)$$

where: q_{eq} is the amount of lead adsorbed at equilibrium (mg/g), q_t is the amount of lead adsorbed at time t (mg/g), and k_2 is the pseudo-second-order rate constant (g/mg min). In this case, the pseudo-second-order model provided an excellent fit to the experimental data, with a correlation coefficient $R^2 = 0.9999$ (Table 1). The calculated equilibrium adsorption capacity $q_{eq} = 93.45$ mg/g closely matched the experimental value, confirming the validity of the model. The rate constant $k_2 = 0.0071$ g/mg min indicates that chemisorption is the primary controlling step, involving the ion exchange or sharing of electrons between Pb ions and the active functional groups on the KOS surface, which is the dominant mechanism. The Weber-Morris intraparticle diffusion model was applied to evaluate whether diffusion into the pores of the biosorbent particles was a limiting factor in the adsorption process. The Weber-Morris model is represented by the equation:

$$q_t = K_{id} t^{0.5} + C \quad (4)$$

where: K_{id} is the intraparticle diffusion rate constant mg/g·min^{1/2}, and C is the intercept, which indicates the boundary layer thickness.

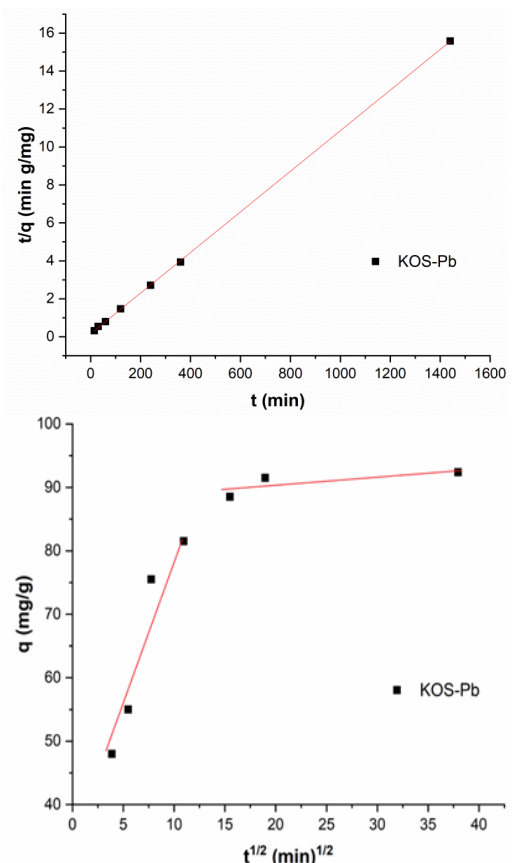


Fig.5: Kinetic models of Pb adsorption on KOS

The plot of q_t versus $t^{1/2}$ (Figure 5) revealed two distinct linear regions, indicating a multi-stage adsorption process. During the initial phase, the adsorption was dominated by surface interactions, as indicated by the first linear segment with a k_{id1} value of 3.5512 mg/g·min^{1/2} and an intercept $C_1 = 27.9739$ mg/g. In the later stages, the adsorption slowed down, with a lower $k_{id2} = 0.14901$ mg/g·min^{1/2} suggesting that intraparticle diffusion became a more significant factor.

The results from the Weber-Morris model suggest that while external surface adsorption controls the initial rate of lead removal, intraparticle diffusion plays a role in the later stages of the process (Simić et al., 2022). However, the non-zero intercepts indicate that intraparticle diffusion is not the sole rate-limiting step. This finding supports the conclusion that the adsorption process is primarily controlled by chemisorption, with diffusion processes contributing to the overall mechanism (Dimitrijević et al., 2023).

Table 1: Kinetic parameters of Pb adsorption on KOS

Adsorbent KOS	KOS-Pb
$q_{eq, exp}$ [mg/g]	92.45±0.71
Pseudo-First-Order Model	
$q_{eq, cal}$ [mg/g]	87.49±0.84
k_1 [1/min]	8.95±0.25
R^2	0.9503 ±0.086
Pseudo-Second-Order Model	
$q_{eq, cal}$ [mg/g]	93.45±0.38
k_2 [g/mg min ⁻¹]	0.0071±0.0017
R^2	0.9999±0.0001
Weber-Morris diffusion Model	
k_{id1} [mg/g min ^{-1/2}]	3.5512 ±0.032
C_1 [mg/g]	27.9739 ±0.014
R^2	0.9173 ±0.022
k_{id2} [mg/g min ^{-1/2}]	0.14901 ±0.0124
C_2 [mg/g]	86.8698 ±1.251
R^2	0.8527 ±0.0671

3.3. Adsorption of Lead on a Modified Biosorbent: Isotherm

The adsorption behavior of Pb onto a KOS was analyzed using multiple isotherm models to elucidate the underlying adsorption mechanisms. These models, including Langmuir (Langmuir, 1918), Freundlich (Freundlich, 1907), Sips (Sips, 1948), and Redlich-Peterson (Peterson and Redlich, 1962), each offered insights into different aspects of the adsorption. They provided Figure 6. perspectives on whether adsorption followed a monolayer or multilayer formation, the surface homogeneity of the biosorbent, and the possible coexistence of physical and chemical adsorption.

Langmuir isotherm is based on the assumption that adsorption occurs uniformly on a monolayer across a homogeneous surface, where all active sites have the same energy and each site can adsorb only one ion. This isotherm model is expressed as follows:

$$q_e = q_{max} K_L C_e / (1 + K_L C_e) \quad (5)$$

Where: q_e is the equilibrium adsorption capacity (mg/g), q_{max} is the maximum adsorption capacity (mg/g), K_L is the Langmuir constant (L/mg), and C_e is the equilibrium concentration of lead ions (mg/L).

In this study, the maximum adsorption capacity q_{max} was determined to be 191.41 mg/g, with a Langmuir constant $K_L = 0.0072$ L/mg (Table 2). This relatively high q_{max} value indicates that the KOS has a substantial capacity to remove Pb, reflecting a favorable interaction between Pb ions and the surface functional groups. Additionally, the high R^2 value of 0.9647

suggests that the Langmuir model fits the experimental data well, supporting the idea of monolayer adsorption (Table 2) which is characteristic of chemisorption. The favorability of this adsorption process is further confirmed by the dimensionless separation factor $R_L = 0.970$ (Table 2), indicating that adsorption is most favorable at lower Pb concentrations.

Table 2: Isotherm parameters for Pb²⁺ adsorption on KOS

Models	Parameters	KOS-Pb
Langmuir	q_m (mg/g)	191.41±2.15
	K_L (L/mg)	0.0072±0.0016
	R^2	0.9647±0.0021
	R_L	0.970±0.014
	χ^2	44.34 ±0.08
Freundlich	K_F (mg/g)(L/mg) ^{1/n}	5.63±1.18
	1/n	1.78±0.24
	R^2	0.9442±0.0127
	χ^2	96.76±1.59
Sips	q_m (mg/g)	178.21±1.98
	K_S (L/mg)	0.0644±0.0125
	n_s	0.99±0.14
	R^2	0.9016±0.14
Redlich-Peterson	χ^2	227.46±0.23
	K_{RP} (L/g)	1.158±0.305
	a_{RP} (L/mg)	8.53±0.21
	β	1.33±0.67
	R^2	0.9777±0.0313
	χ^2	51.82±0.45

$$R_L = \frac{1}{1 + K_L C_0} \quad (6)$$

Freundlich isotherm describes adsorption on a heterogeneous surface, where different sites exhibit varying affinities for the adsorbate. It is represented by the following equation:

$$q_e = K_F C_e^{1/n} \quad (7)$$

Where: K_F is the Freundlich constant, 1/n indicates the intensity of adsorption, with 1/n < 1 suggesting favorable adsorption.

In this study, the Freundlich constant K_F was 5.63, and the parameter 1/n = 1.78, indicating that the adsorption process was moderately favorable and occurred on a heterogeneous surface (Table 2). The $R^2 = 0.9442$ value was slightly lower than for the Langmuir model, suggesting that although the surface is somewhat heterogeneous, the assumption of monolayer adsorption remains more appropriate.

The Sips isotherm is a hybrid model that combines features of both the Langmuir and Freundlich isotherms. It predicts Freundlich behavior at lower concentrations and Langmuir behavior at higher concentrations. The Sips equation is:

$$q_e = q_{max} (K_S C_e)^{1/ns} / (1 + (K_S C_e)^{1/ns}) \quad (8)$$

where: q_{max} is the maximum adsorption capacity, K_S is the Sips constant, and ns is the heterogeneity factor.

The Redlich-Peterson isotherm is an empirical model that combines elements of both the Langmuir and Freundlich models, making it suitable for systems involving both monolayer and multilayer adsorption. The equation is:

$$q_e = K_{RP} C_e / (1 + a_{RP} C_e^g) \quad (9)$$

where: K_{RP} and a_{RP} represent Redlich-Peterson constants (L/g), and ((mg/L)^{-g}), respectively, and g is an empirical Redlich-Peterson parameter ($g \leq 1$)

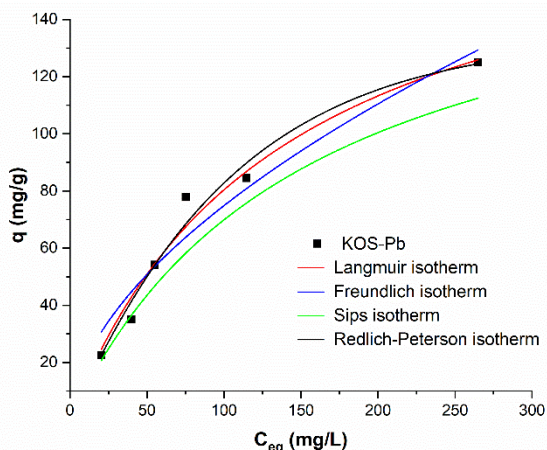


Fig.6: Adsorption isotherms of Pb removal on KOS

The Redlich-Peterson model provided the best fit to the experimental data, with an $R^2 = 0.9777$ (Table 2). The parameters were $K_{RP} = 1.158$ L/g, $a_{RP} = 8.53$ L/mg, and $g = 1.33$, suggesting that chemisorption plays a significant role in the adsorption process, though physical adsorption may also contribute at higher concentrations. This is in accordance with the Kinetic study.

The strong performance of the Redlich-Peterson model, as indicated by its high R^2 value, suggests that this model effectively captures the complexity of the adsorption process. The g parameter points to a combination of chemisorption and physical adsorption, with chemisorption being the dominant mechanism.

As can be concluded from results, the KOS demonstrates better adsorption properties for Pb removal compared to similar materials available in literature (Table 3).

Table 3. Adsorption capacity of different sorbents towards Pb(II) ions

Adsorbent	q_m (mg/g)	Reference
	Pb(II)	
Phoenix dactylifera	5.15	(Yazid and Maachi, 2008)
Black cumin seeds biochar	17.70	(Birgili et al., 2024)
Carbons derived of chestnut kernel	27.53	(Momčilović, 2012)
Carbon derived of Black pine cones	25.51	(Momčilović, 2012)
Simplicillium chinense QD10	57.80	(Torres, 2020)
<i>Pseudomonas</i> sp.	60.00	(Kaleem et al., 2023)
Rice husk biochar	72.00	(Birgili et al., 2024)
Nostoc sp. MK-11	83.96	(Kaleem et al., 2023)
Olive cake biochar	102.00	(Birgili et al., 2024)
<i>Sargassum</i> sp.	112.00	(Putri et al., 2021)
Lemna minor	142.86	(Kaya et al., 2024)
<i>Allium scorodoprasum</i> L.	190.41	(Senol and Arslanoğlu, 2024)
KOS	191.41	This study
OS	38.00	This study

3.4. Ion-exchange mechanism

The ion exchange mechanism plays a crucial role in the adsorption of heavy metal ions from aqueous solutions. In this study, the removal of Pb ions was investigated in relation to the release of cations (Ca^{2+} , Na^+ , K^+ , and Mg^{2+}) from the biosorbent surface during the adsorption process. The results, indicate that with increasing Pb concentration, there is a corresponding release of Ca^{2+} , Na^+ , K^+ , and Mg^{2+} ions from the biosorbent, confirming that ion exchange is one of the mechanisms in-

involved in the adsorption process (Figure 7). The higher release of Ca^{2+} , followed by K^+ and Mg^{2+} , indicates that calcium and potassium play a more significant role in the ion-exchange process, while sodium shows relatively minor participation. The exchange of these cations for Pb ions supports the formation of ionic bonds between the biosorbent surface and the lead ions (Petrović et al., 2016; Simić et al., 2022). The results also suggest that the quantity of released cations is lower than the total amount of adsorbed Pb^{2+} ions, indicating that additional mechanisms, such as surface complexation or chemisorption, may also contribute to the overall removal process.

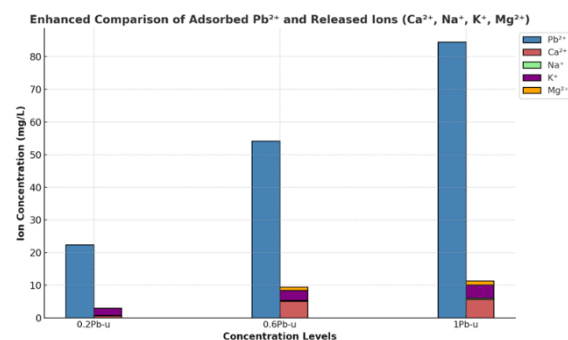


Fig.7: Ion exchange of M^{2+} during the Pb adsorption on KOS

4. CONCLUSION

This study successfully demonstrated that the modification of OS with KOH significantly enhances its adsorption capacity for Pb^{2+} from contaminated water. The chemical modification increased the surface area and exposed functional groups that improved the interaction with pollutants, leading to a substantial increase in adsorption efficiency. The pseudo-second-order kinetic model confirmed that chemisorption was the primary mechanism involved. Langmuir isotherm model revealed a maximum adsorption capacity of 191.41 mg/g. The results indicate that KOS is a highly effective biosorbent for Pb removal, offering a solution to both water pollution and agricultural waste management. Its application can be further expanded to other environmental contaminants, providing a scalable, eco-friendly option for wastewater treatment.

ACKNOWLEDGMENTS

This work was supported by the Ministry of Science, Technological Development and Innovation of the Republic of Serbia (Contract No. 451-03-66/2024-03/200023 and 451-03-65/2024-03/200135).

CONFLICT OF INTEREST

The authors declare that they have no financial or commercial conflict of interest.

REFERENCES

- Babicka, M., Woźniak, M., Bartkowiak, M., Peplińska, B., Waliszewska, H., Zborowska, M., Borysiak, S., and Ratajczak, I. (2022): Miscanthus and Sorghum as sustainable biomass sources for nanocellulose production, *Industrial Crops and Products*, **186**, 115177. <https://doi.org/10.1016/j.indcrop.2022.115177>
- Birgili, B., Haykiri-Acma, H., and Yaman, S. (2024): Biosorption of lead, hexavalent chrome and cadmium from aqueous solution by torrefied biomass, *International Journal of Environmental Science and Technology*, **21**(12), 8049–8062. <https://doi.org/10.1007/s13762-024-05507-w>

- Borrega, M., Hinkka, V., Hörhammer, H., Kataja, K., Kenttä, E., Ketoja, J. A., Palmgren, R., Salo, M., Sundqvist-Andberg, H., and Tanaka, A. (2022): Utilizing and Valorizing Oat and Barley Straw as an Alternative Source of Lignocellulosic Fibers, *Materials*, **15**(21), 7826. <https://doi.org/10.3390/ma15217826>
- Bryngelsson, S., Dimberg, L. H., and Kamal-Eldin, A. (2002): Effects of Commercial Processing on Levels of Antioxidants in Oats (*Avena sativa* L.), *Journal of Agricultural and Food Chemistry*, **50**(7), 1890–1896. <https://doi.org/10.1021/jf011222z>
- Dehkhoda, S., Bagheri, M., Heydari, M., and Rabieh, S. (2022): Extraction of carboxylated nanocellulose from oat husk: Characterization, surface modification and in vitro evaluation of indomethacin drug release, *International Journal of Biological Macromolecules*, **212**, 165–171. <https://doi.org/10.1016/j.ijbiomac.2022.05.125>
- Dimitrijević, J., Jevtić, S., Marinković, A., Simić, M., Koprivica, M., and Petrović, J. (2023): Ability of Deep Eutectic Solvent Modified Oat Straw for Cu(II), Zn(II), and Se(IV) Ions Removal, *Processes*, **11**(5), 1308. <https://doi.org/10.3390/pr11051308>
- Dong, J., Cai, F., Shen, R., and Liu, Y. (2011): Hypoglycaemic effects and inhibitory effect on intestinal disaccharidases of oat beta-glucan in streptozotocin-induced diabetic mice, *Food Chemistry*, **129**(3), 1066–1071. <https://doi.org/10.1016/j.foodchem.2011.05.076>
- Fan, L., Miao, J., Yang, J., Zhao, X., Shi, W., Xie, M., Wang, X., Chen, W., An, X., Luo, H., Ma, D., and Cheng, L. (2022): Invasive plant-crofton weed as adsorbent for effective removal of copper from aqueous solution, *Environmental Technology & Innovation*, **26**, 102280. <https://doi.org/10.1016/j.eti.2022.102280>
- Freundlich, H. (1907): Über die Adsorption in Lösungen, *Zeitschrift Für Physikalische Chemie*, **57U**(1), 385–470. <https://doi.org/10.1515/zpch-1907-5723>
- Gollakota, A. R. K., Subbaiah Munagapati, V., Shu, C.-M., and Wen, J.-C. (2022): Adsorption of Cr (VI), and Pb (II) from aqueous solution by 1-Butyl-3-methylimidazolium bis(trifluoromethylsulfonyl)imide functionalized biomass Hazel Sterculia (*Sterculia Foetida* L.), *Journal of Molecular Liquids*, **350**, 118534. <https://doi.org/10.1016/j.molliq.2022.118534>
- Gómez Aguilar, D. L., Rodríguez Miranda, J. P., Astudillo Miller, M. X., Maldonado Astudillo, R. I., and Esteban Muñoz, J. A. (2020): Removal of Zn(II) in Synthetic Wastewater Using Agricultural Wastes, *Metals*, **10**(11), 1465. <https://doi.org/10.3390/met10111465>
- Hatiya, N. A., Reshad, A. S., and Negie, Z. W. (2022): Chemical Modification of Neem (*Azadirachta indica*) Biomass as Bioadsorbent for Removal of Pb²⁺ Ion from Aqueous Waste Water, *Adsorption Science & Technology*, **2022**, 7813513. <https://doi.org/10.1155/2022/7813513>
- Ho, Y. S., and McKay, G. (1999): Pseudo-second order model for sorption processes, *Process Biochemistry*, **34**(5), 451–465. [https://doi.org/10.1016/S0032-9592\(98\)00112-5](https://doi.org/10.1016/S0032-9592(98)00112-5)
- Jovanović, A., Stevanović, M., Barudžija, T., Cvijetić, I., Lazarević, S., Tomašević, A., and Marinković, A. (2023): Advanced technology for photocatalytic degradation of thiophanate-methyl: Degradation pathways, DFT calculations and embryotoxic potential, *Process Safety and Environmental Protection*, **178**, 423–443. <https://doi.org/10.1016/j.psep.2023.08.054>
- Kaleem, M., Minhas, L. A., Hashmi, M. Z., Ali, M. A., Mahmoud, R. M., Saqib, S., Nazish, M., Zaman, W., and Samad Mumtaz, A. (2023): Biosorption of Cadmium and Lead by Dry Biomass of Nostoc sp. MK-11: Kinetic and Isotherm Study, *Molecules*, **28**(5), 2292. <https://doi.org/10.3390/molecules28052292>
- Kaya, S., Çetinkaya, S., Jalbani, N. S., Yenidünya, A. F., Küçük, N., Kasaka, E., and Maslov, M. M. (2024): Biosorption of lead ions (Pb²⁺) from water samples using dried *Lemna minor* biomass: experimental and density functional theory studies, *Biomass Conversion and Biorefinery*, **14**(15), 17603–17617. <https://doi.org/10.1007/s13399-023-03914-6>
- Kim, I.-S., Hwang, C.-W., Yang, W.-S., and Kim, C.-H. (2021): Multiple Antioxidative and Bioactive Molecules of Oats (*Avena sativa* L.) in Human Health, *Antioxidants*, **10**(9), 1454. <https://doi.org/10.3390/antiox10091454>
- Kosiorek, M., and Wyszczkowski, M. (2019): Content of macronutrients in oat (*Avena sativa* L.) after remediation of soil polluted with cobalt, *Environmental Monitoring and Assessment*, **191**(6), 389. <https://doi.org/10.1007/s10661-019-7529-6>
- Kubovský, I., Kačíková, D., and Kačík, F. (2020): Structural Changes of Oak Wood Main Components Caused by Thermal Modification, *Polymers*, **12**(2), 485. <https://doi.org/10.3390/polym12020485>
- Lagergren, S. (1898): Zur theorie der sogenannten adsorption gelöster stoffe, **24**, 1–39. <https://doi.org/10.1007/BF01501332>
- Lai, P., Zhou, H., Niu, Z., Li, L., Zhu, W., and Dai, L. (2023): Deep eutectic solvent-mediated preparation of solvothermal carbon with rich carboxyl and phenol groups from crop straw for high-efficient uranium adsorption, *Chemical Engineering Journal*, **457**, 141255. <https://doi.org/10.1016/j.cej.2022.141255>
- Langmuir, I. (1918): The adsorption of gases on plane surfaces of glass, mica and platinum, *Journal of the American Chemical Society*, **40**(9), 1361–1403. <https://doi.org/10.1021/ja02242a004>
- Lawal, I. A., Chetty, D., Akpotu, S. O., and Moodley, B. (2017): Sorption of Congo red and reactive blue on biomass and activated carbon derived from biomass modified by ionic liquid, *Environmental Nanotechnology, Monitoring & Management*, **8**, 83–91. <https://doi.org/10.1016/j.enmm.2017.05.003>
- Momčilović, M. Z. (2012): *Kinetic and equilibrium parameters of adsorption processes under removal of certain harmful cationic ingredients from aqueous solutions using activated carbons derived by thermochemical treatment of chestnut kernel and Black pine cones*, PhD thesis, Prirodno-Matematički Nis.
- Peterson, D. L., and Redlich, O. (1962): Sorption of Normal Paraffins by Molecular Sieves Type 5A., *Journal of Chemical & Engineering Data*, **7**(4), 570–574. <https://doi.org/10.1021/je60015a043>
- Petrović, J., Ercegović, M., Simić, M., Kalderis, D., Koprivica, M., Milojković, J., and Radulović, D. (2023): Novel Mg-doped pyrohydrochars as methylene blue adsorbents: Adsorption behavior and mechanism, *Journal of Molecular Liquids*, **376**, 121424. <https://doi.org/10.1016/j.molliq.2023.121424>
- Petrović, J., Stojanović, M., Milojković, J., Petrović, M., Šoštarić, T., Laušević, M., and Mihajlović, M. (2016): Alkali modified hydrochar of grape pomace as a perspective adsorbent of Pb²⁺ from aqueous solution, *Journal of Environmental Management*, **182**, 292–300. <https://doi.org/10.1016/j.jenvman.2016.07.081>
- Putri, L. S. E., Syafiq, E., and Apriliyani, E. (2021): Biosorption of lead by biomass of dried sargassum, *IOSR Journal of Environmental Science, Toxicology and Food Technology (IOSR-JESTFT)*, **15**(4), 58–63.
- Ren, Y., Yang, X., Niu, X., Liu, S., and Ren, G. (2011): Chemical Characterization of the Avenanthramide-Rich Extract from Oat and Its Effect on D-Galactose-Induced Oxidative Stress in Mice, *Journal of Agricultural and Food Chemistry*, **59**(1), 206–211. <https://doi.org/10.1021/jf103938e>
- Şenol, Z. M., and Arslanoğlu, H. (2024): Influential biosorption of lead ions from aqueous solution using sand leek (*Allium scorodoprasum* L.) biomass: kinetic and isotherm study, *Biomass Conversion and Biorefinery*. <https://doi.org/10.1007/s13399-024-05539-9>
- Simić, M., Petrović, J., Šoštarić, T., Ercegović, M., Milojković, J., Lopičić, Z., and Kojić, M. (2022): A Mechanism Assessment and Differences of Cadmium Adsorption on Raw and Alkali-Modified Agricultural Waste, *Processes*, **10**(10), 1957. <https://doi.org/10.3390/pr10101957>
- Sips, R. (1948): On the Structure of a Catalyst Surface, *The Journal of Chemical Physics*, **16**(5), 490–495. <https://doi.org/10.1063/1.1746922>
- Torres, E. (2020): Biosorption: A Review of the Latest Advances, *Processes*, **8**(12), 1584. <https://doi.org/10.3390/pr8121584>
- Weber, W. J., and Morris, J. C. (1963): Kinetics of Adsorption on Carbon from Solution, *Journal of the Sanitary Engineering Division*, **89**(2), 31–59. <https://doi.org/10.1061/JSEDAI.0000430>
- Yazid, H., and Maachi, R. (2008): Biosorption of Lead (II) Ions From Aqueous Solutions by Biological Activated Dates Stems, *Journal of Environmental Science and Technology*, **1**(4), 201–213. <https://doi.org/10.3923/jest.2008.201.213>
- Ying, D., Hlaing, M. M., Lerisson, J., Pitts, K., Cheng, L., Sanguansri, L., and Augustin, M. A. (2017): Physical properties and FTIR analysis of rice-oat flour and maize-oat flour based extruded food products containing olive pomace, *Food Research International*, **100**, 665–673. <https://doi.org/10.1016/j.foodres.2017.07.062>
- Zhang, T., Jiang, W., Cao, Y., Zhu, C., Toukouki, S., and Yao, S. (2022): A facile one-pot synthesis of ionic liquid@porous organic frameworks for rapid high-capacity removal of heavy metal ions, pesticides and aflatoxin from two non-food bioactive products, *Industrial Crops and Products*, **181**, 114859. <https://doi.org/10.1016/j.indcrop.2022.114859>